geoconvention
Virtual Event
September 13 - 15
2021

Geomechanical characterization of proppant embedment behaviours in Montney siltstone using laboratory tests

Wenbo Zheng, University of Northern British Columbia
Albert Cui, AGAT Laboratories

Summary

A series of laboratory tests were conducted on achieved samples that were originally cored from a Montney well at a depth of 2068-2270 m. Brinell indentation tests were used to quantify the resistance of the siltstone rock to indentation. Proppant embedment tests were conducted to investigate the mechanical response of a monolayer proppant pack sandwiched between two rock surfaces under a triaxial loading. The results show that the Montney siltstone has Brinell hardness values ranging from 59 to 117 HBW, averaging at 76.8 ± 13.4 HBW. The Young's modulus interpreted from the Brinell hardness tests ranges from 17.6 to 78.1 GPa, averaging at 42.0 GPa that is consistent with compression test results. The initial fracture aperture propped by a monolayer of proppant is around 0.37 mm with 0.25-0.30 mm diameters proppant but is highly variable with 0.5-0.6 mm diameters proppant (>0.65 mm). Most of the proppant particles remained unbroken at 40 MPa thus the decrease in fracture aperture mainly results from proppant deformation and proppant embedment into the rock faces. Using the average particle force acting on a proppant particle to calculate the proppant deformation and embedment seems to be consistent with the laboratory results.

Method

The tested samples are Montney siltstone obtained from the unconventional Montney play in British Columbia, Canada (Cui and Brezovski 2013, Gensterblum et al. 2015, Ghanizadeh et al. 2015). Twenty two Disk-shaped samples were indented with a Tungsten carbide indenter with a spherical 1 mm diameter tip using a MetaRock testing system (Figure). The samples were mold with epoxy in proper position and were polished to have a smooth surface. All the samples were first tested as received under ambient conditions. The indenter was perpendicularly brought into contact with the sample surface under a contact load of 20 mN. The force was increased up to 35 N and then unloaded to 0 N under a constant loading rate of 17.5 N/min. The force and the indentation depth were recorded during the test. Nine locations (three by three) were indented for each sample.

Small diameter cores were drilled from slabs and were further sub-cored to take approximate 1-inch diameter by 2-inch long cylindrical plugs. Cylindrical-shaped samples were tested under ambient condition using a GCTX RTX-3000 testing system. Samples were mounted in the testing vessel and the axial and radial deformations were measured, respectively, with two LDVTs and one LDVT. The testing procedure for a proppant embedment test is shown in Figure 2. First, a triaxial test was performed on a sample to get the elastic properties of the sample with an axial stress of 40 MPa and a confining stress of 20 MPa. Second, the sample was split along the cross-section into two smaller cylindrical cores (denoted as A and B, each approximately 1-inch diameter with a 1-inch length). One layer of proppants (monolayer) was placed between the two split cylindrical cores to form a proppant pack. Finally, the whole sandwiched-sample was

subjected to the same triaxial testing with an axial stress of 40 MPa and a confining pressure of 20 MPa.

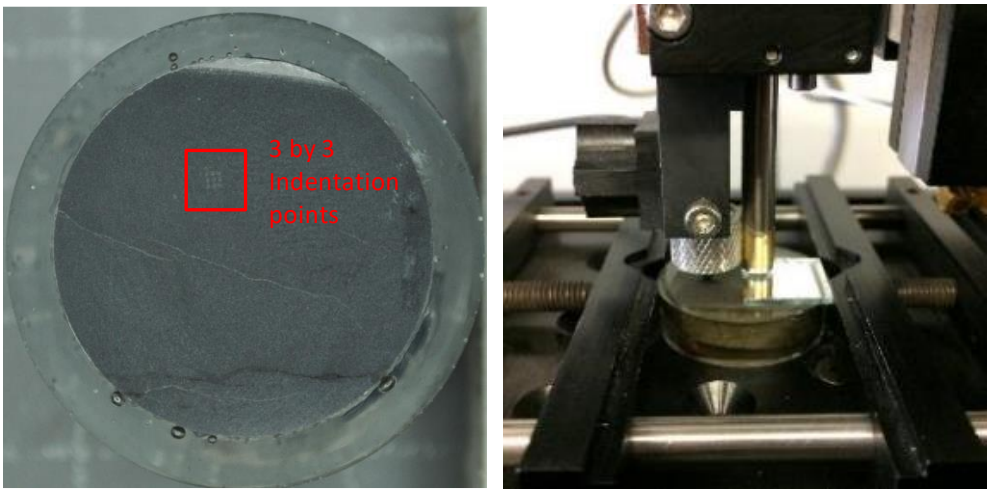

Figure 1. Sample (left) and indenter (right) for Brinell hardness test

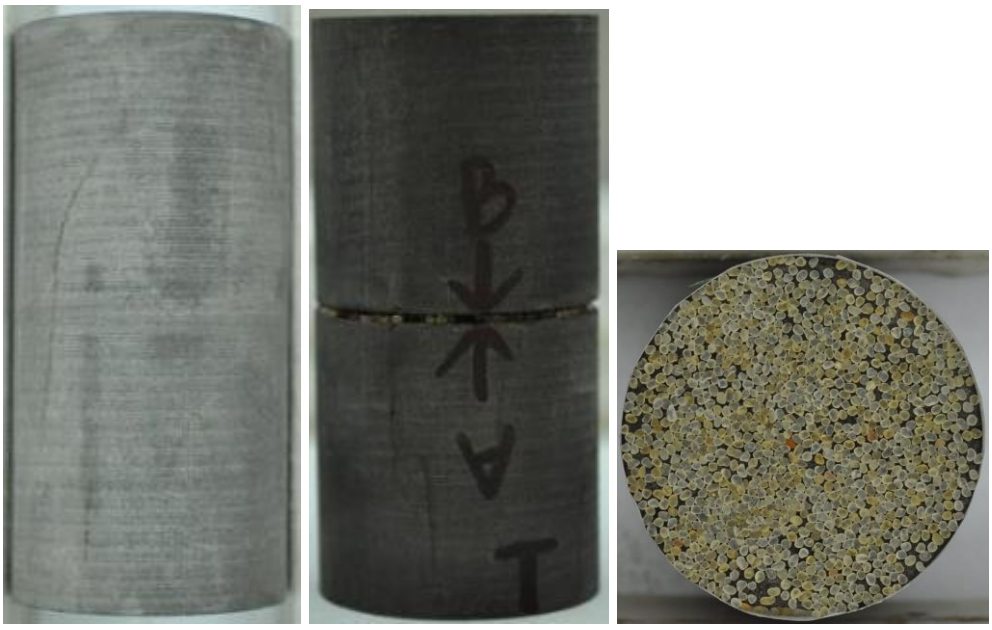

Figure 2. (a) intact sample for elastic triaxial test; (b) sample split to two halves for proppant embedment test; (c) monolayer of proppants between two split halves

Ten proppant embedment tests with two different proppant sizes (0.5-0.6 mm denoted as G500 and 0.25-0.3 mm denoted as G250) of two different proppant types (Jordan sand and a ceramic proppant) were conducted. After placing a proppant pack between two rock cores, the initial fracture aperture prior to loading was determined as the difference between the total length of a

sample with proppants and the length of the sample without proppants. The placement of proppant grains between two split halves are shown in Fig. 2. The mass of proppants ranges from 0.173 to 0.422 g, which corresponds a proppant pack loading ranging from 0.07 to 0.17 lb/ft2 over a circular cross section with a diameter of 2.54 mm. The initial fracture apertures propped by ceramic proppants are slightly higher than those propped by Jordan sand when using the same particle size.

Results and Conclusions

Figure 3(a) shows nine force-indentation curves from the same rock sample. The determination of Brinell hardness and local Young's modulus follows a procedure detailed in Zheng et al. (2020). It can be seen that the hardness and Young's modulus vary greatly across the span of the sample depth from 2068.12 to 2337.39 m MD. The maximum indentation depth at a 35 N indentation force ranges from 9.7 to 19.2 μm. The value of Brinell hardness ranges from 59 to 117 HBW. The Young's modulus interpreted from the Brinell hardness tests ranges from 17.6 to 78.1 GPa, with an average of 42.0 GPa and a standard deviation of 14.8 GPa. The average value of Young's modulus is close to those from the triaxial compressive tests. The relatively large deviation in Young's modulus and Brinell hardness may be due to the inhomogeneity of rock along different depths and under a small scale.

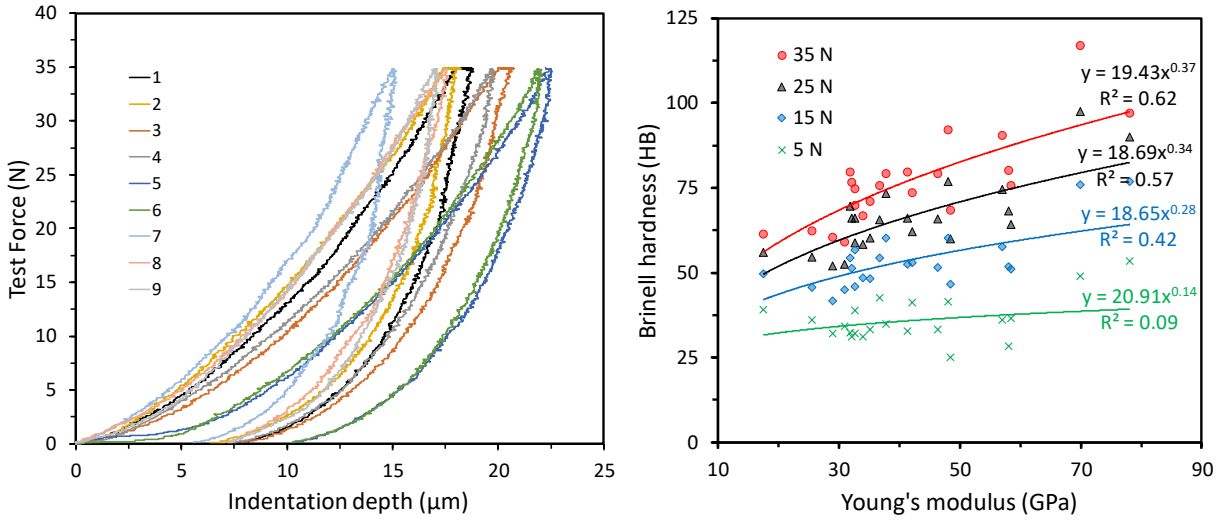

Figure 3. (a) Force-indentation curves; (b) correlation between Young's modulus and Brinell hardness using indentation depth under different indentation loads

Figure 3(b) shows the correlations between the Brinell hardness values and the Young's modulus values calculated from the hardness tests for different indentation forces. Note that the Brinell hardness changes with the indentation force, as the relation between indentation force and depth is not linear, especially at the initial loading stage with low indentation forces. The correlations between the Brinell hardness values and the Young's modulus values are more positive at higher indentation forces compared with those at lower indentation forces.

After placing a proppant pack between two rock cores, the initial fracture aperture prior to loading was determined as the difference between the total length of a sample with proppants and the length of the intact sample without proppants. Typically, the axial displacement of intact samples without proppants and samples sandwiched with proppants increase close to linearly with an increase in confining pressure and axial stress. The fracture aperture reduction due to isostatic confining was calculated by subtracting the axial deformation of the intact sample during isostatic confining from the axial deformation of the sample sandwiched with proppants during isostatic confining. Likewise, the fracture aperture reduction due to axial loading was calculated in a similar manner.

The results of proppant embedment tests The initial fracture aperture has a thickness ranging from 0.927 to 0.338 mm. Proppants with G500 size typically result in a higher fracture aperture than that with G250 proppants. For proppant packs using G500 size, large variation in the initial fracture aperture was observed and the initial fracture aperture was > 0.65 mm. For proppant packs using G250 size, the initial fracture aperture was around 0.37 mm except for sample TWN2-15. This sample (TWN2-15) had an initial fracture aperture of 0.645 mm that is likely due to the uneven proppant distribution forming a multi-layers proppant pack between the core surfaces. Note that for the sample TWN1-13 the membrane was found broken during the embedment triaxial test thus this set of data was excluded in the following analysis. The reduction in the fracture aperture by an isostatic confining stress of 20 MPa ranges from 0.045 to 0.174 mm, while the aperture reduction by an axial stress of 40 MPa (20 MPa deviatoric stress + 20 MPa confining pressure) ranges from 0.018 to 0.119 mm. The final remaining fracture aperture ranges from 0.433 to 0.605 mm with G500 proppants, and ranges from 0.192 to 0.263 mm with G250 proppants. Most proppant remained unbroken after the proppant embedment test

Table 1. Evolution of proppant-propped fracture aperture in embedment tests

Sample ID	Siltstone Young's modulus (GPA)	Proppant		Fracture aperture (mm)			
		Type	Mass (g)	F_0	F_1	F_2	F_3
TWN1-13	62.5	G500 Jordan	0.364	0.927	0.377	0.031	0.519
TWN1-15	43.1	G500 ceramic	0.363	0.711	0.115	0.019	0.577
TWN2-13	41.1	G500 Jordan	0.422	0.650	0.099	0.119	0.433
TWN2-15	40.0	G250 Jordan	0.185	0.645	0.052	0.041	0.552
TWN2-17	38.0	G500 ceramic	0.302	0.754	0.087	0.063	0.605
TWN2-19	36.1	G250 ceramic	0.173	0.338	0.079	0.067	0.192
TWN3-10	42.2	G500 Jordan	0.390	0.658	0.045	0.090	0.523
TWN3-12	45.4	G250 Jordan	0.187	0.352	0.114	0.018	0.220

TWN3-17	38.9	G500 ceramic	0.408	0.681	0.174	0.025	0.482
TWN3-19	39.8	G250 ceramic	0.173	0.389	0.062	0.064	0.263

F0 – initial fracture aperture
F1 – fracture aperture reduction by isostatic confining pressure
F2 - fracture aperture reduction by deviator stress
F3 – remain fracture aperture

As most proppants remained intact after the proppant embedment tests, the fracture aperture reduction under axial compression during the tests should mainly result from proppant deformation and proppant embedment into the rock surface without considering other factors. Here the proppant particle number between the two fractures for each embedment test was estimated based on the proppant mass and density, based on which the average force acting on each particle was calculated as shown in **Error! Reference source not found.** 2. The particle force for G500 proppant is from 11.1 to 16.4 N, while that for G250 is from 3.1 to 3.6 N. This average particle force was used to estimate the proppant embedment and proppant deformation between the fractures as shown in **Error! Reference source not found.**.

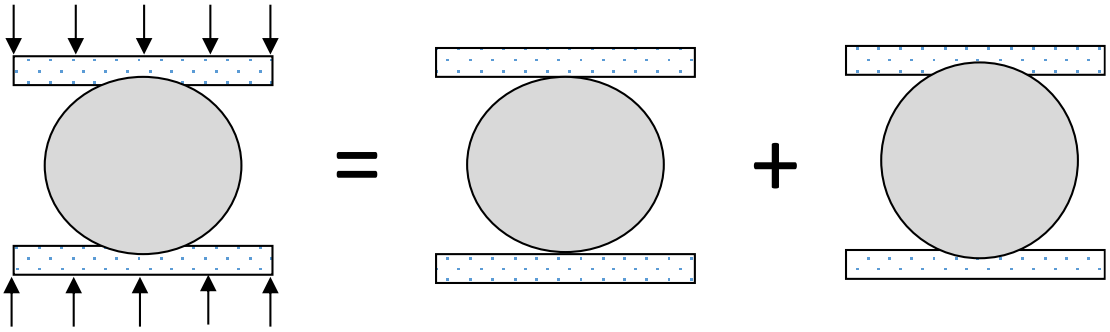

Figure 4. Reduction in propped fracture aperture caused by proppant deformation and embedment

The proppant deformation between two rock faces can be expressed as (Cundall and Strack 1979):

$$P_1 = \frac{2F_p}{k_n} = \frac{2F_p}{\pi RE} \tag{1}$$

where F_p is the particle force, k_n is the particle stiffness that is related to the particle radius, R, and the particle-particle effective modulus, E, which were 1.1 GPa and 2.2 GPa for Jordan sand and ceramic proppants, respectively.

The embedment depth of proppants into fracture surfaces during a proppant embedment test can be roughly estimated using Equation 2. Note that the Brinell hardness was determined from the known Young's modulus (Table 1) following the equations in Figure 3(b).

$$P_2 = \frac{F_p}{9.80665\pi D_i HB} \tag{2}$$

Table 2. Interpretation of propped fracture aperture during embedment test (40 MPa)

Sample ID	Proppant			HB (HBW)	Fracture aperture (mm)					
	Type	Particle number	Particle force/N		P_0	P_1	P_2	P_3	F_3 (lab)	P_2/D (%)
TWN1-13	G500 Jordan	1577	12.9	57.8	0.55	0.027	0.026	0.497	0.519	4.7
TWN1-15	G500 ceramic	1483	13.7	51.7	0.55	0.014	0.031	0.504	0.577	5.6
TWN2-13	G500 Jordan	1828	11.1	46.5	0.55	0.023	0.028	0.498	0.433	5.1
TWN2-15	G250 Jordan	6411	3.2	35.7	0.275	0.013	0.021	0.241	0.552	7.6
TWN2-17	G500 ceramic	1234	16.4	53.6	0.55	0.017	0.036	0.496	0.605	6.5
TWN2-19	G250 ceramic	5654	3.6	34.9	0.275	0.008	0.024	0.243	0.192	8.7
TWN3-10	G500 Jordan	1689	12.0	48.4	0.55	0.025	0.029	0.495	0.523	5.3
TWN3-12	G250 Jordan	6480	3.1	36.8	0.275	0.013	0.020	0.242	0.220	7.3
TWN3-17	G500 ceramic	1667	12.2	47.5	0.55	0.013	0.030	0.507	0.482	5.5
TWN3-19	G250 ceramic	5654	3.6	35.7	0.275	0.008	0.024	0.244	0.263	8.7

P0 – predicted initial fracture aperture
P1 – predicted proppant deformation
P2 – predicted proppant embedment
P3 – predicted remaining fracture aperture

The results of the predicted final fracture aperture after proppant deformation and embedment at 40 MPa are compared against the laboratory results shown in **Error! Reference source not found.**. It seems that the predicted fracture apertures are consistent with the measurements from the proppant embedment tests excluded those possibly inaccurate measurements for samples TWN1-15, TWN2-15, TWN2-17, and TWN3-19. At 40 MPa, the proppant deformation is 0.023-0.027 mm for G500 Jordan sand, 0.013-0.017 mm for G500 ceramic proppant, 0.013 mm for G250 Jordan sand, and 0.008 mm for G250 ceramic proppant. The proppant deformation of G500 is about twice of that of G250 for the same type of proppants, while the proppant deformation of Jordan sand is about twice of that of ceramic for the same proppant size. For proppant embedment, a lower Brinell hardness value was used for rock samples with G250 size proppant particles than G500 size because of smaller particle forces acting on rock surfaces. The proppant embedment of different samples ranges from 0.020 to 0.036 mm. Except for G500 Jordan sand, the proppant embedment is typically larger than the proppant deformation at 40 MPa, especially for G250 proppants.

Acknowledgements

This work was support by grants from Mitacs and the British Columbia Oil and Gas Commission. Trican Geological Solutions (now AGAT Laboratories) contributed to the laboratory measurement work.

References

1. Cui, A. and Brezovski, R., 2013, November. Laboratory permeability measurements of unconventional reservoirs: useless or full of information. In A Montney Example From The Western Canadian Sedimentary Basin. SPE 167047 presented at the Unconventional Resources Conference, Brisbane, Australia (pp. 11-13).
2. Gensterblum, Y., Ghanizadeh, A., Cuss, R.J., Amann-Hildenbrand, A., Krooss, B.M., Clarkson, C.R., Harrington, J.F. and Zoback, M.D., 2015. Gas transport and storage capacity in shale gas reservoirs–A review. Part A: transport processes. Journal of Unconventional Oil and Gas Resources, 12, pp.87-122.
3. Ghanizadeh, A., Clarkson, C.R., Aquino, S., Ardakani, O.H. and Sanei, H., 2015. Petrophysical and geomechanical characteristics of Canadian tight oil and liquid-rich gas reservoirs: II. Geomechanical property estimation. Fuel, 153, pp.682-691.
4. Zheng, W., Tannant, D.D., Cui, X., Xu, C. and Hu, X., 2020. Improved discrete element modeling for proppant embedment into rock surfaces. Acta Geotechnica, 15(2), pp.347-364.
5. Cundall, P.A. and Strack, O.D., 1979. A discrete numerical model for granular assemblies. Geotechnique, 29(1), pp.47-65.